



Cascade trailing-edge noise modeling using a mode-matching technique and the edge-dipole theory



Michel Roger^a, Benjamin François^a, Stéphane Moreau^{b,*}

^a *École Centrale de Lyon, Laboratoire de Mécanique des Fluides et Acoustique, UMR CNRS 5509, 36 avenue Guy de Collongue, 69134 Ecully, France*

^b *Dept. Génie Mécanique, Sherbrooke University, Québec, Canada J1K 2R1*

ARTICLE INFO

Article history:

Received 4 January 2016

Received in revised form

11 June 2016

Accepted 27 June 2016

Handling Editor: P. Joseph

Available online 16 July 2016

Keywords:

Aeroacoustics

Fan trailing-edge noise

ABSTRACT

An original analytical approach is proposed to model the broadband trailing-edge noise produced by high-solidity outlet guide vanes in an axial turbomachine. The model is formulated in the frequency domain and first in two dimensions for a preliminary assessment of the method. In a first step the trailing-edge noise sources of a single vane are shown to be equivalent to the onset of a so-called edge dipole, the direct field of which is expanded in a series of plane-wave modes. A criterion for the distance of the dipole to the trailing-edge and a scaling of its amplitude is defined to yield a robust model. In a second step the diffraction of each plane-wave mode is derived considering the cascade as an array of bifurcated waveguides and using a mode-matching technique. The cascade response is finally synthesized by summing the diffracted fields of all cut-on modes to yield upstream and downstream sound power spectral densities. The obtained spectral shapes are physically consistent and the present results show that upstream radiation is typically 3 dB higher than downstream radiation, which has been experimentally observed previously. Even though the trailing-edge noise sources are not vane-to-vane correlated their radiation is strongly determined by a cascade effect that consequently must be accounted for. The interest of the approach is that it can be extended to a three-dimensional annular configuration without resorting to a strip theory approach. As such it is a promising and versatile alternative to previously published methods.

© 2016 Elsevier Ltd. All rights reserved.

1. Introduction

The design of many axial-flow fan stages involves a rotor and a downstream row of stationary outlet guide vanes called stators as shown in Fig. 1. The aerodynamic noise of the rotor–stator stage is caused by various aerodynamic interactions, all responsible for unsteadiness of the velocity relative to the blades/vanes. According to Ffowcs Williams and Hawkings' acoustic analogy and for subsonic Mach numbers, sound mainly originates from the fluctuating lift forces that result from this unsteadiness, all acting as equivalent dipoles [1].

The main manifestation of this generic mechanism is the wake-interaction noise produced as the wakes of the rotor blades impinge on the stator vanes. The mean velocity deficit and the turbulence in the wakes generate tonal noise and broadband noise, respectively, the sources of which are distributed on the vanes. Similarly, stationary inflow distortions and ingested turbulence at inlet are the origin of tonal and broadband noise generated by the rotor blades. Independently the

* Corresponding author.

Nomenclature			
a	constant	V	vane number
\bar{a}_j, a_j	pressure and potential coefficients for plane waves	v_x	acoustic axial velocity
A_m^j, B_s^j	transmitted and reflected mode amplitudes, single interface	\mathbf{v}_K^h	hydrodynamic velocity associated to the Kutta condition
c	chord length	(x, y)	axial and transverse Cartesian coordinates
c_0	sound speed	$X = x/\beta$	scaled coordinate
D_m^0, U_m^0	downstream and upstream mode amplitudes in the channels	α_s^j	scattered transverse wavenumbers of transmitted/reflected waves
E, F	Fresnel integral and related function	$\beta = \sqrt{1 - M_0^2}$	compressibility parameter
h	inter-vane channel height	Γ	pressure and axial-velocity vector
$k = \omega/c_0$	acoustic wavenumber	δ_1	displacement thickness
$K = k/\beta$	scaled wavenumber	ϕ	acoustic potential
$K^{(j)}$	axial wavenumber in the channels	Φ_{pp}	wall-pressure power spectral density
K_m	incident axial wavenumber	Ψ_{pp}	dimensionless wall-pressure power spectral density
\bar{K}_s^j	effective axial wavenumbers of reflected/transmitted waves	ρ_0	fluid density
ℓ_y	wall-pressure spanwise coherence length	σ	constant
L	vane spanwise extent	ω	angular frequency
M_0	axial Mach number	$\bar{\omega}$	dimensionless angular frequency
p, p_0	acoustic pressure	Ω_K	vorticity vector generated by the Kutta condition
r_c	radius of the unwrapped cut of the stator	<i>Subscripts and superscripts</i>	
$(r_0, \theta_0), (r, \theta)$	source and observer cylindrical coordinates around an edge	$(-)_0$	source-point coordinate
$(\bar{r}_0, \bar{\theta}_0), (\bar{r}, \bar{\theta})$	same coordinates corrected for convection	$(-)^0$	reference channel
\bar{R}	corrected source-to-observer distance	$(-)_j$	incident wave index
R_s, T_s	reflected and transmitted mode amplitudes, double interface	$(-)_m$	channel mode index
R_1, R_2	hub and tip radii	$(-)_K$	Kutta-condition associated quantity
t	time	$(-)_s$	reflected or transmitted wave index
U_r, U_a	inlet and outlet velocities of a stator vane	$(-)_{i,r,t,u,d}$	incident, reflected, transmitted, upstream and downstream potentials
U_0	reference freestream velocity	$(-)^{\pm}$	for downstream/upstream wavenumbers

turbulent boundary layers developing on the blades and the vanes are scattered as sound at the trailing edges, also contributing to the broadband noise. Finally secondary flows such as tip-leakage vortices generate their own unsteadiness and associated noise. The aforementioned trailing-edge noise sources are not blade-to-blade or vane-to-vane correlated, which means that the sound is generated in the same way as for an isolated airfoil. But the sound radiation away from the trailing-edge area is more or less dramatically restructured by multiple scattering on adjacent blades/vanes. This restructuration referred to as the cascade effect is the main motivation of the present work. The emphasis is on the trailing-edge noise of the stator, though the same approach could be transposed to a rotor as explained later on.

In most architectures such as depicted in Fig. 1 the outlet guide vanes are moderately cambered and staggered at leading edge, and nearly parallel to the axis at trailing edge. Indeed they are designed to restore an axial mean flow of speed U_a from the incident swirl produced by the rotor and emphasized by the oblique relative speed of magnitude U_r in the figure. As a result the vanes have a large overlap and can be viewed from downstream as an array of parallel and zero-stagger plates. When trying to reproduce aeroacoustic phenomena using analytical approaches, the cascade effect of the stator appears as a key feature to deal with. The cascade effect is not only involved in the sound generation process but also when the sound generated by the rotor blades is transmitted downstream in the exhaust duct, especially for stators with a large number of vanes and quite large hub-to-tip ratios R_1/R_2 . Many studies contributed to the development of analytical or semi-analytical cascade response functions for sound generation or transmission in blade rows [2–24]. The approach developed by Glegg [15] and later improved by Posson et al. [23] is selected here for the discussion. But only wake-interaction noise or turbulence-impingement noise is generally considered. The cascade effect on the trailing-edge noise mechanism is more difficult to formulate even though an attractive and elegant approach has been proposed by Glegg and Jochault [25]. The issue is that trailing-edge noise sources are localized and poorly correlated, which makes them difficult to describe in a cascade context. Though only outlet guide vanes are considered in the present work, the same would hold for the blades of a rotor except that most often the overlap is smaller, at least in the tip region of the blades, and that the number of blades is also smaller. Furthermore the stagger angle of the blades is quite large. The case of the stator is chosen here because the

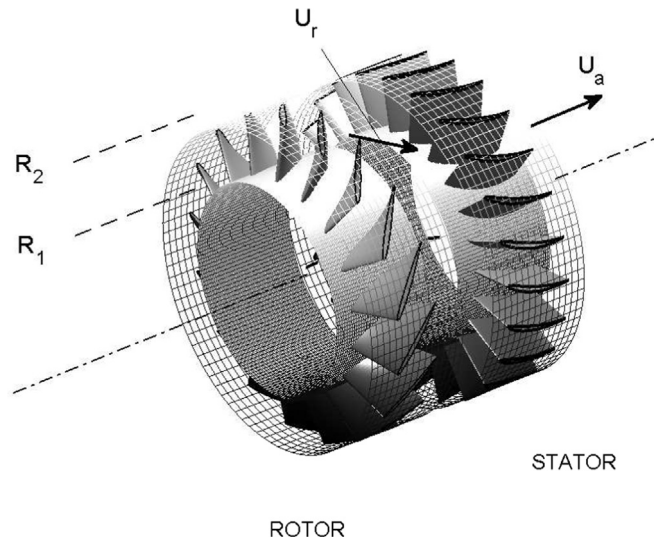


Fig. 1. Typical axial-flow fan architecture. (R_1, R_2): hub and tip radii, U_r : oblique relative velocity on the stator leading edge, U_a : axial flow velocity at outlet.

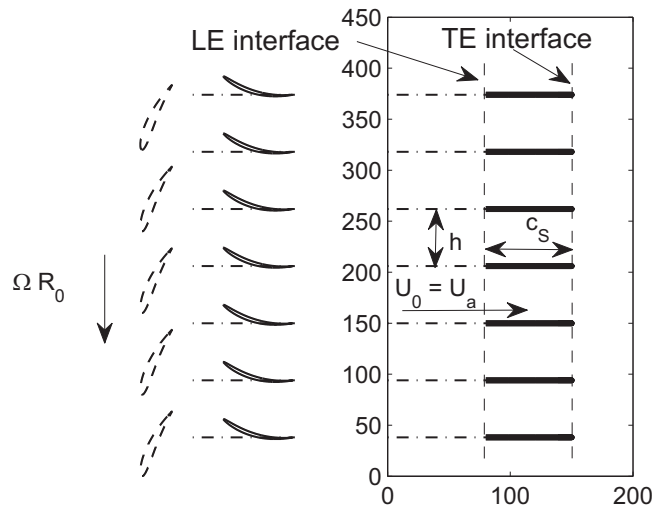


Fig. 2. Unwrapped representation of a stator as an equivalent infinite rectilinear cascade of plates, in arbitrary Cartesian coordinates. Cylindrical cut of radius R_0 . Rotor blades featured in dashed lines.

equivalent cascade can be more reasonably assumed with zero stagger, both for the sake of simplicity and for the sake of demonstrating the feasibility of a new approach. As will be pointed out in several instances later on in the text, the approach can be extended quite easily to more realistic configurations; this however is beyond the scope of the paper.

The aforementioned approach by Glegg [15], Glegg and Jochault [25] and Posson et al. [23] relies on an extensive use of the Wiener–Hopf technique formulated in a Cartesian reference frame for a rectilinear cascade. This means that the investigated annular cascade must be split into a series of thin annuli that are unwrapped and treated separately. Arbitrary stagger angle, sweep and lean can be accounted for by changing the parameters in each strip. In contrast no simple equivalent in cylindrical coordinates is available and as a result adjacent blades or vanes are artificially considered as parallel plates. The present approach is proposed as an alternative. It is based on a mode-matching technique, considering a blade/vane row as a periodic array of bifurcated waveguides. It can be transposed in a three-dimensional context in cylindrical coordinates for the analysis of annular cascades. This versatility is an attractive advantage since the splitting of a machine into strips is avoided, but it is balanced by the limitation that blade/vane twist or other design features cannot be simply considered. The two-dimensional extension to staggered vanes is straightforward as suggested by similar works in electromagnetic wave theory [26]. Finally the Wiener–Hopf technique and the mode-matching technique are mathematically equivalent when addressing rigid-plate cascade problems in two dimensions. But one or the other is presumably better suited depending on the design features that must be preserved when three-dimensional blade/vane rows are modeled.

The present investigation remains two-dimensional as in the preliminary study by Roger et al. [27] but it must be understood as the first step of a methodology that will be progressively generalized and implemented in a unified three-dimensional model of axial-flow turbomachine. The stator vanes are assumed parallel, axially aligned and zero-stagger plates (Fig. 2). They are equivalent to a periodic array of bifurcated waveguides with rigid walls. As a principle, it is stated that the trailing-edge noise sources of an isolated vane can be reproduced by introducing an equivalent lift dipole very close to the trailing edge from downstream, the direct field of which is diffracted by the edge. This intuition is a key step of the approach. Its validity is confirmed in Section 2.1 and is guided by the fact that trailing-edge noise physics develops in the very vicinity of the trailing edge and radiates waves of opposite phases on both sides of the plate. The equivalent excitation of the trailing-edge interface of the stator in terms of acoustic plane-wave modes is derived in Section 2.2. The response of the stator as a waveguide system is then addressed for isolated incident modes and for the complete field of the trailing-edge dipole in Section 3, where fundamental scattering properties are discussed. Finally the application of the methodology to predict power spectra of the broadband trailing-edge noise is introduced in Section 4, where an indicative statistical model of the hydrodynamic wall-pressure is used as input.

2. Edge-dipole formulation

2.1. Expression of the equivalent dipole

The underlying interpretation of the proposed model is that cascade trailing-edge noise radiation can be formulated as an equivalent upstream-to-downstream sound-transmission problem that will be solved using a mode-matching procedure. In this view an incident acoustic excitation of the stator is defined, following the intuition that the trailing-edge noise sources of an isolated vane can be reproduced with an equivalent point dipole approaching the edge from downstream at a very close distance. Therefore key points of the model are to justify the relevance of this dipole and to determine its strength from the basic knowledge of the sound generating mechanism. Trailing-edge noise results from the scattering of boundary-layer turbulence as sound at the trailing edge under the effect of the Kutta condition. Various interpretations have been proposed in the literature, most of which were reviewed by Howe [28]. Though a complete discussion is out of the scope of the present work, some points can be retained. Following the original statement of Lighthill's analogy the sources of the sound can be considered equivalent quadrupoles essentially defined by the velocity fluctuations distributed in the immediate vicinity of the trailing-edge, including the boundary-layer and the near wake. These quadrupoles experience scattering by the edge, leading to specific sound radiation. In view of the involved fluid scales in the boundary-layer the edge is equivalently considered as a semi-infinite rigid plate. The properties of the sound field are explained by the asymptotic behavior of the associated Green's function, referred to as the half-plane Green's function, for sources located at very short distances to the edge with respect to the acoustic wavelengths. This view was first exposed in a pioneering work by Ffowcs Williams and Hall [29], ignoring the effect of the mean flow. The asymptotic analysis shows that the amplitude of the sound field is strongly amplified with respect to what the quadrupoles would radiate in free field, by a factor $(kr_0)^{-1}$ if r_0 is the distance to the edge and k the acoustic wavenumber, and that the directivity is a cardioid pattern with zero sound in the wake and a maximum sound in the opposite direction. The radiated field also exhibits opposite phases on both sides of the half-plane. Amiet's formulation of trailing-edge noise [30] is also cited here as an alternative interpretation rather based on Ffowcs Williams and Hawkins's statement of the analogy [31]. According to it the boundary-layer turbulence is considered *via* its pressure trace. That trace, of hydrodynamic nature, is forced to zero at the trailing-edge by the Kutta condition, generating an additional pressure jump distributed on the wall and concentrated at the trailing-edge. This pressure jump radiates as equivalent dipoles. Both interpretations must be equivalent and should provide similar results if applied correctly, even if they rely on different quantities, turbulent velocity and hydrodynamic fluctuating pressure, respectively. Amiet's model is currently used to predict the trailing-edge noise of isolated thin airfoils and has been proven to be accurate when fed with reliable wall-pressure statistical data [32]. In its original form the sound radiation is calculated by an integral of the pressure jump distribution over the actual chord length whereas the derivation of the induced pressure jump assumes a semi-infinite plate. Therefore performing the integration up to infinity upstream in Amiet's model produces the same aforementioned cardioid pattern. This confirms the identity of both interpretations.

An essential point is that as soon as the asymptotic regime of the half-plane Green's function is entered the cardioid pattern with phase opposition is obtained for any dipole or quadrupole source, irrespective of its exact location or orientation (except for some very restrictive conditions [33]); in other words it is not imposed by the source physics but by Green's function itself. This suggests that an equivalent single lift dipole located downstream of the trailing-edge in the continuation of the wall and at a very small distance can be used, quite arbitrarily, to describe the sources of trailing-edge noise. The normal orientation of the lift dipole is chosen for simplicity and its downstream location is essential for the mode-matching procedure. Now its exact distance to the edge is a free parameter; the smaller it is the weaker the strength of the dipole must be, as a result of the amplification, so that a constant wall-pressure trace is ensured. In fact the final tuning of the dipole is achieved by comparing the acoustic wall-pressure distribution obtained from Green's function on the half-plane to the induced pressure jump in Amiet's model.

The field of the dipole in the presence of the half-plane is derived from the exact two-dimensional half-plane Green's function in the presence of flow, introduced by Jones [34] and re-addressed by Rienstra [35]. Only the transverse component of the first gradient of Green's function with respect to source coordinates is needed because the dipole of interest is

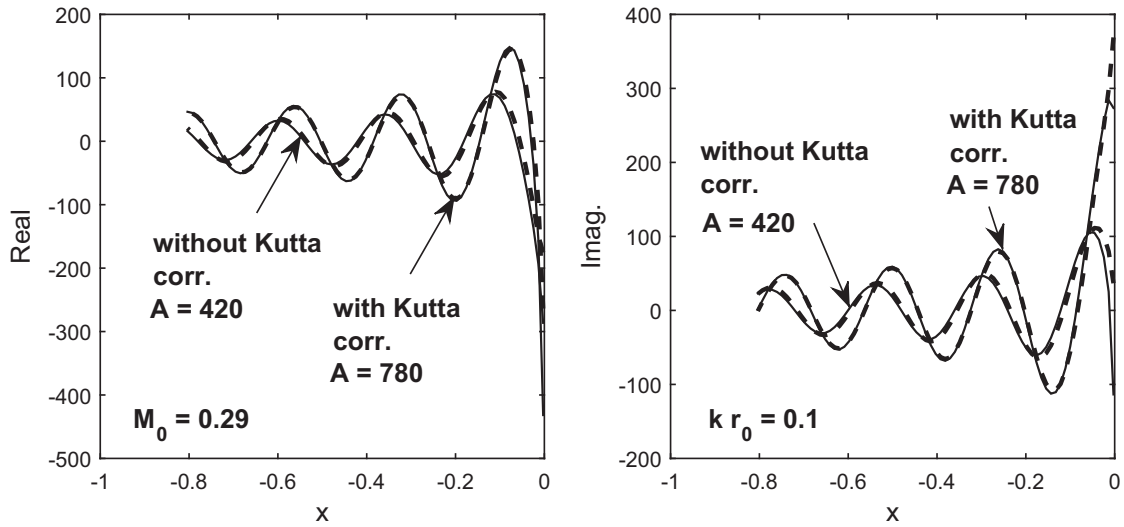


Fig. 3. Real and Imaginary parts of the radiating wall pressure. Amiet's solution (thin cont.), edge scattering of a point dipole (thick dashed), with and without Kutta condition. Phase tuning factor: $e^{-0.2i\pi/4}$ (Kutta) and $e^{i\pi/4}$ (no Kutta).

oriented normal to the flow direction. If no additional Kutta condition is imposed at the edge Green's function reads, for a flow of Mach number M_0 in the positive x direction

$$G_M(x, y, k) = \frac{1}{\beta} e^{-iKM(x-X_0)} G^{(1/2)}(X, y, K)$$

with

$$G^{(1/2)}(X, y, K) = \int_{-\infty}^{s_1} e^{iK\bar{r}_1\sqrt{1+u^2}} \frac{du}{\sqrt{1+u^2}} + \int_{-\infty}^{s_2} e^{iK\bar{r}_2\sqrt{1+u^2}} \frac{du}{\sqrt{1+u^2}} \tag{1}$$

In this expression $\bar{r}_{1,2}^2 = \bar{r}^2 + \bar{r}_0^2 - 2\bar{r}\bar{r}_0 \cos(\bar{\theta} \mp \bar{\theta}_0)$, with $\bar{r} = \sqrt{X^2 + y^2}$ being the corrected observer distance to the edge involving the stretched coordinate $X = x/\beta$, with $\beta = \sqrt{1 - M_0^2}$, and $K = k/\beta$. The angles $\bar{\theta}$ and $\bar{\theta}_0$ are defined as the corrected angles from the wake direction $x > 0$, and

$$s_1 = \frac{2\sqrt{\bar{r}_0\bar{r}}}{\bar{r}_1} \cos \frac{\bar{\theta} - \bar{\theta}_0}{2}, \quad s_2 = -\frac{2\sqrt{\bar{r}_0\bar{r}}}{\bar{r}_2} \cos \frac{\bar{\theta} + \bar{\theta}_0}{2}.$$

Though it admits a simplified expression for a point source approaching the edge in such a way that $k\bar{r}_0$ takes arbitrary small values, the exact implementation has been used here. The equivalent dipole is set at zero θ_0 angle. Only the trace of the pressure field at the wall is needed in the present study. It is plotted as the thick dashed line in Fig. 3 for a Mach number of 0.29 and a source-to-edge Helmholtz number of 0.1. It is worth noting that Jones [34] and Rienstra [35] also consider an optional Kutta condition in the form of the additional correcting term

$$G_K(x, y, k) = \frac{A_K}{2} \frac{e^{i\pi/4}}{\sqrt{\pi}} e^{-iK\bar{r}} \left[F\left(\sqrt{2K\bar{r}} \sin \frac{\bar{\theta} - \bar{\theta}_1}{2}\right) + F\left(\sqrt{2K\bar{r}} \sin \frac{\bar{\theta} + \bar{\theta}_1}{2}\right) \right] - \frac{A_K}{2} 2e^{-iKX/M_0} \cosh\left(\frac{\beta K}{M_0} y\right) H(-y) \tag{2}$$

where the factor A_K is given by Jones as

$$\frac{A_K}{2} = \text{sign}(y_0) \sqrt{\frac{2\pi}{K\bar{r}_0}} \sqrt{1 - \frac{X_0}{\bar{r}_0}} \sqrt{\frac{M_0}{1 + M_0}} e^{-iK\bar{r}_0 - i\pi/4}$$

and where $\bar{\theta}_1$ is an imaginary angle such that $\cos \bar{\theta}_1 = 1/M_0$. H is the Heaviside function and F is the complex function of complex argument defined by

$$F(z) = e^{iz^2} \int_z^\infty e^{-it^2} dt = \frac{\sqrt{\pi}}{2} e^{-i\pi/4} e^{iz^2} \text{erfc}\left(e^{i\pi/4} z\right).$$

This correction is known to cause amplification of the radiated field for very small values of $k\bar{r}_0$ and significant values of the Mach number [36]. The complete result including it is also plotted for completeness in Fig. 3, where a phase shift is noticed with respect to the no-Kutta solution.

Amiet's formulation of trailing-edge noise in the frequency domain [30,37] provides directly an expression for the radiating wall-pressure produced by the primary scattering of boundary-layer vorticity into sound at the edge. This pressure field must be distinguished from the incident hydrodynamic pressure associated with the convected turbulence in the boundary layers. The latter is the origin of the former but does not enter the problem statement explicitly. Assuming an infinite chord, that pressure is distributed according to the expression

$$P_1(x) = \bar{A}e^{i\alpha K_1 X} [(1-i)E(-[\alpha K_1 + (1+M_0)\mu]X) - 1] \tag{3}$$

if the same convention $e^{-i\omega t}$ is chosen everywhere for monochromatic waves. Eq. (3) refers to the two-dimensional response for a single gust or Fourier component of the incident hydrodynamic pressure, of complex amplitude \bar{A} . α , estimated here around 1.25, is the flow-speed to convection-speed ratio, $K_1 = \omega/(\beta U_0)$ is a modified aerodynamic wavenumber and $\mu = K_1 M_0/\beta$. E is the Fresnel integral defined as

$$E(\xi) = \int_0^\xi \frac{e^{it}}{\sqrt{2\pi t}} dt.$$

$\bar{A} = Ae^{i\varphi}$ is a scaling parameter used to make the expression of Eq. (3) coincide at best with the field calculated from Eq. (1) by adjusting the amplitude A and the phase φ . The tuned Amiet's solution is plotted as the thin continuous lines in Fig. 3, where it is found in a good agreement with the trace of the equivalent point dipole. For the test the amplitude 470 is used with a phase factor $e^{i\pi/4}$ to fit with the no-Kutta solution and the amplitude 780 with a phase factor $e^{-0.2i\pi/4}$ to fit with the solution including the Kutta correction. In fact in a statistical declination of Amiet's trailing-edge noise model the amplitude of the edge dipole would be imposed by the gust amplitude A in Amiet's formulation. The latter would be related to the hydrodynamic wall-pressure spectrum taken closely upstream of the trailing-edge and to its spanwise correlation length [38]. The phase φ would play no role. The result confirms that a point dipole can indeed be used to accurately describe the sources of trailing-edge noise.

2.2. Expression of the excitation

The direct sound field radiated from a point lift-dipole is also given by the scalar product of the dipole strength with the first gradient of the free-space Green's function with respect to the source coordinates. In the two-dimensional space of the study, Green's function is expressed with the Hankel function. For a unit dipole strength the field reads

$$\frac{\partial G}{\partial y_0} = \frac{ik(y_0 - y)}{4\beta\bar{R}} e^{-iKM_0 X} H_0^{(1)'}(K\bar{R}) = \frac{iK(y - y_0)}{4\bar{R}} e^{-iKM_0 X} H_1^{(1)}(K\bar{R})$$

where (x_0, y_0) and (x, y) stand for source and observer coordinates, respectively. $R = [(x - x_0)^2 + (y - y_0)^2]^{1/2}$ is the source to observer distance and \bar{R} its expression with X instead of x . In the present case the trailing edge of a reference vane is located at the origin of coordinates. Because the unwrapped representation of the annular stator at radius r_c must be periodic of period Vh where V is the number of vanes and $h = 2\pi r_c/V$ is the channel width, the same point source must be repeated every V channels. This leads to the periodized field

$$p_0 = \frac{iK}{4} e^{-iKM_0 X} \sum_{n=-\infty}^{\infty} \frac{y + nVh}{[X^2 + (y + nVh)^2]^{1/2}} H_1^{(1)} \left(K [X^2 + (y + nVh)^2]^{1/2} \right) \tag{4}$$

This two-dimensional field can be expanded as an infinite discrete set of oblique plane-wave modes in the form

$$p_0 = e^{-iKM_0 X} \sum_{j=-\infty}^{\infty} \bar{a}_j^\pm e^{i(K_{xj}X + K_{yj}y)} \tag{5}$$

with

$$K_{yj} = \frac{j2\pi}{Vh}, \quad K_{xj} = \pm \left[K^2 - \left(\frac{j2\pi}{Vh} \right)^2 \right]^{1/2}.$$

Indeed each plane wave must also be periodic in the y direction with the period Vh . The $+$ sign holds for propagation in the downstream direction ($x > 0$), the $-$ sign for the upstream direction ($x < 0$). A true plane wave is obtained only if K_{xj} is real and positive, which corresponds to the cut-on condition $K > j2\pi/(Vh)$. Otherwise the mode is said cut-off and the necessary condition of exponential decay is ensured by putting

$$K_{xj} = \pm i \left[\left(\frac{j2\pi}{Vh} \right)^2 - K^2 \right]^{1/2}.$$

Downstream propagation is considered first. Identifying both expressions of p_0 and making use of the orthogonality integrals of exponential modes leads to the expression of \bar{a}_j^+ as

$$\bar{a}_j^+ = \frac{iK}{4Vh} e^{-i[K^2 - (j2\pi/(Vh))^2]^{1/2} X}$$

$$\begin{aligned} & \times \sum_{n=-\infty}^{\infty} \int_0^{Vh} \frac{y+nVh}{[X^2+(y+nVh)^2]^{1/2}} H_1^{(1)}\left(K[X^2+(y+nVh)^2]^{1/2}\right) e^{-ij2\pi y/(Vh)} dy \\ & = \frac{iK}{4Vh} e^{-i[K^2-(j2\pi/(Vh))^2]^{1/2}X} \int_{-\infty}^{\infty} \frac{tH_1^{(1)}\left(K\sqrt{X^2+t^2}\right)}{\sqrt{X^2+t^2}} e^{-ij2\pi t/(Vh)} dt. \end{aligned}$$

The antisymmetric part of the integrand can be ignored since it integrates to zero. Integrating by parts then leads, after a further change of variable, to the simplified form

$$\bar{a}_j^+ = \frac{j\pi X}{(Vh)^2} e^{-i[K^2-(j2\pi/(Vh))^2]^{1/2}X} \int_0^{\infty} H_0^{(1)}\left(KX\sqrt{1+u^2}\right) \cos\left(\frac{j2\pi X}{Vh}u\right) du.$$

The integral is readily calculated by using the connection between $H_0^{(1)}$ and the modified Bessel function K_0 such that [39]

$$K_0(-i\xi) = \frac{i\pi}{2} H_0^{(1)}(\xi)$$

and the result [40]

$$\int_0^{\infty} K_0\left(\alpha\sqrt{\xi^2+\beta^2}\right) \cos\gamma\xi d\xi = \frac{\pi}{2\sqrt{\alpha^2+\gamma^2}} e^{-\beta\sqrt{\alpha^2+\gamma^2}} \tag{6}$$

valid for complex numbers α and β of positive real parts and for any real number γ . Finally the coefficient is found as

$$\bar{a}_j^+ = \frac{j\pi}{(Vh)^2} \left[K^2 - \left(\frac{j2\pi}{Vh}\right)^2 \right]^{-1/2}. \tag{7}$$

As expected the expression does not depend on the coordinate x , which is ensured by a proper choice of the square root in Eq. (6). For the coefficient \bar{a}_j^- the developments are the same except that x is negative and that now the $-$ sign is taken for K_{xj} . Since X can be replaced by $|X|$ in the integrals the same expression is found in the end, so that $\bar{a}_j^- = \bar{a}_j^+ = \bar{a}_j$. This is also expected from the upstream/downstream symmetry of the sources in the absence of flow. Eq. (7) for the upstream-propagating waves allows defining a relevant excitation of the trailing-edge interface of a stator. Because they are plane waves, the classical matching procedure for two-dimensional bifurcated waveguides [41] applies, whatever the cut-on or cut-off conditions might be.

Instantaneous pressure fields as calculated from Eq. (4) with the infinite sum of Hankel functions and from the sum of plane-wave modes with the coefficients of Eq. (7) are compared in Fig. 4. The instantaneous pressure field, identical for both, is illustrated in Fig. 4a, where the dipoles corresponding to the repetitions of a single trailing-edge source are indicated by the white circles and arrows. In this map and all subsequent maps in the paper the light and dark spots correspond to negative and positive deviations from the mean pressure. The flow is from left to right and the flat plates mimicking the vanes are not shown since the figure only deals with the direct field of the dipoles. The periodicity Vh is that of the unwrapped circular cut of the stator. Away from the near-field region surrounding the line of dipoles and not paying attention to the interference fringes, the sound field is of overall uniform amplitude in both directions. In contrast higher pressure fluctuations are seen in the vicinity of the sources. This is expected since the field is made of cut-off modes discernable close to the sources and cut-on modes which propagate without attenuation. A typical pressure profile along the line $y=0.08$ is plotted in Fig. 4b, where the continuous line stands for the sum of Hankel functions and the dashed line for

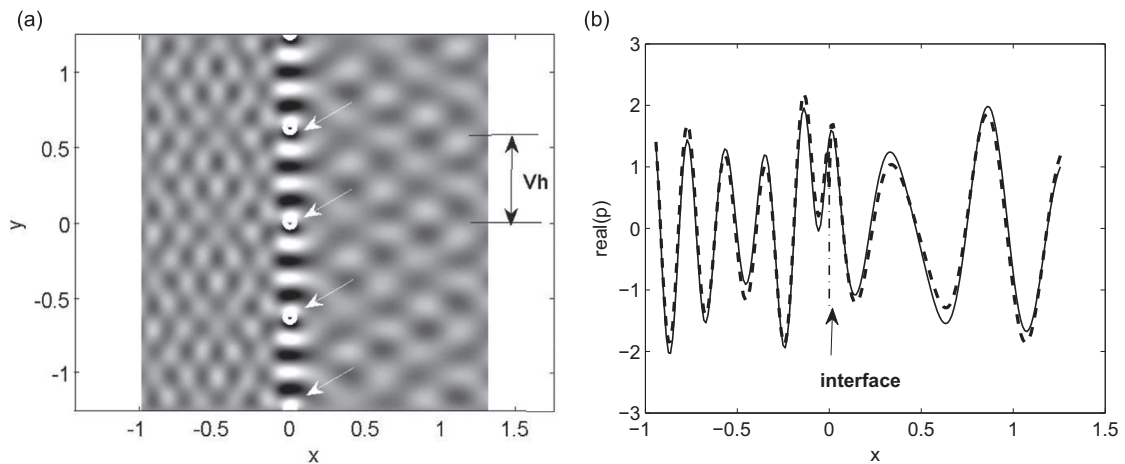


Fig. 4. (a) Simulated instantaneous sound pressure produced by a series of point dipoles indicated by arrows; (b) pressure profiles predicted with the sum of Hankel functions (plain) and with the sum of plane waves (dashed). Helmholtz number $kVh = 17.4$, $U_0 = 100$ m/s.

the sum of plane-wave modes. The agreement confirms that the plane-wave expansion is relevant and can be used for the mode-matching technique. Moreover a large number of Hankel terms are needed to converge in Eq. (4) (300 in the present example) whereas a much smaller number of plane-wave modes are sufficient to reach the same convergence (with few differences between 10 and 30 terms). Yet residual discrepancies attributed to sum truncations, not prejudicial for the present application, are seen in the figure. The smaller number of required plane waves is in favor of the present model and can be explained as follows. The Hankel functions are the expressions of cylindrical waves but they are not appropriate to reproduce the periodicity in the y -direction. In contrast oblique plane waves already have an inherent periodicity in this direction through the wavenumber K_y in Cartesian coordinates.

It is worth noting that only one lift dipole associated with a single stator vane is needed for the present analysis, because the sources of trailing-edge noise are not vane-to-vane correlated. The present section was aimed at describing the field that this dipole would radiate in the absence of the vanes. The multiple sources in Fig. 4a result from the unwrapped representation of the original 2π -periodicity and correspond to the same vane/dipole.

3. Plane-wave scattering at trailing edge

3.1. General procedure

Once the trailing-edge dipole is defined and its direct field expanded in plane-wave modes, the scattering of each upstream-propagating plane wave by the trailing-edge interface of the stator is calculated using a mode-matching procedure. The theoretical background is found in the literature about bifurcated waveguide systems in a medium at rest, especially in the handbook by Mittra and Lee [41]. The transmission of an acoustic plane wave through an array of zero-stagger parallel plates has also been solved by Linton and Evans [42] in the range of low frequencies for which only the plane-wave mode can propagate inside the individual channels. The formalism has been extended by Ingenito and Roger [43] in the case of semi-infinite channels to account for a uniform fluid motion parallel to the walls and to allow for arbitrary frequencies and higher-order modes in the channels. The extension was used to address some aspects of the upstream sound transmission at the axial inlet of a simplified centrifugal compressor. A further generalization including vortical disturbances as incident waves and a Kutta condition at the trailing edges of a cascade of finite-chord flat plates has also been performed by Bouley et al. [44], dealing with wake-interaction noise generation in axial-flow rotor-stator stages and downstream sound transmission through the stator. The same formulation is used here. It is shortly outlined in this section for the upstream transmission of an isolated oblique acoustic wave through the stator and key steps of the approach are detailed in the Appendix. The complete cascade trailing-edge scattering will be obtained by summing the contributions of all oblique waves defined in Section 2.2.

The developments of the appendix address the initial response of the stator trailing-edge interface disregarding the effect of the leading-edge interface. Multiple higher-order scattered waves must be added following a sequential process to reproduce the complete physical behavior of the cascade. The primary upstream-travelling waves forced in the inter-vane channels are next scattered at the leading-edge interface of the stator. This is accounted for by formulating there another mode-matching problem with the same continuity conditions. Part of the sound is transmitted upstream and part is reflected back in the channels. That part experiences another trailing-edge scattering, which produces transmitted waves downstream and reflected waves in the channels, and so on. Finally four sets of waves are produced, namely open-space waves away from the stator upstream and downstream and internal waves in both directions in the channels. Of course the phase-shift between adjacent channels imposed by the excitation is preserved in the full sound field so that only a single reference channel needs to be considered. The multiple scattering must be reproduced accurately to ensure relevant predictions of the cascade response and to identify possible resonances.

The matching equations are summarized as follows (see details in [44]). The trailing-edge interface is located at $x=c$ where c is the chord length of the vanes and the leading-edge interface is located at $x=0$. The four sets of waves are described by their acoustic potentials: the potentials of the exhaust/reflected and inlet/transmitted waves in the unbounded domains, referred to as ϕ_r and ϕ_t , and those of the upstream and downstream waves in the inter-vane channels referred to as ϕ_u and ϕ_d , respectively. The potential ϕ_r is written as

$$\phi_r = \sum_{s=-\infty}^{+\infty} R_s e^{i\alpha_s y} e^{i\bar{K}_s^+ (X-c/\beta)}, \quad X \geq c/\beta \tag{8}$$

and the potential ϕ_t as

$$\phi_t = \sum_{s=-\infty}^{+\infty} T_s e^{i\alpha_s y} e^{i\bar{K}_s^- X}, \quad X \leq 0, \tag{9}$$

with $\bar{K}_s^\pm = -MK \pm \bar{K}_s^j$.

The potentials ϕ_u and ϕ_d in the reference inter-vane channel are expressed as

$$\phi_u = \sum_{m=0}^{+\infty} U_m^0 \cos\left[\frac{m\pi}{h}y\right] e^{iK_m^- (X-c/\beta)}, \quad \phi_d = \sum_{m=0}^{+\infty} D_m^0 \cos\left[\frac{m\pi}{h}y\right] e^{iK_m^+ X},$$

$$0 \leq X \leq c/\beta, \quad K_m^\pm = -MK \pm K_m. \quad (10)$$

For convenience, a vector Γ_q with the pressure and axial velocity as components is introduced, the indices $q = i, r, t, d, u$ denoting the incident (i), reflected (r), transmitted (t), downstream channel (d) and upstream channel (u) acoustic waves, respectively:

$$\Gamma_q(x, y) = \begin{pmatrix} p(x, y) \\ v_x(x, y) \end{pmatrix}. \quad (11)$$

The continuity of pressure and axial velocity is imposed at the leading-edge interface ($x=0$) and at the trailing-edge interface ($x=c$). The matching equations result as

$$\Gamma_i(c, y) + \Gamma_r(c, y) = \Gamma_d(c, y) + \Gamma_u(c, y), \quad \forall y; \quad (12)$$

$$\Gamma_d(0, y) + \Gamma_u(0, y) = \Gamma_t(0, y), \quad \forall y. \quad (13)$$

The system involves four unknown generic vector variables (\mathbf{R} , \mathbf{D}^0 , \mathbf{U}^0 , \mathbf{T}) and four matching equations. Solving it at once would require the inversion of a large matrix. A sequential method is preferred for the sake of physical understanding. Two distinct matching problems are thus considered, one for each interface, and solved iteratively. In the first step of the iterative procedure the first equation is solved with $\Gamma_d = 0$ and the solution is obtained for Γ_u and Γ_r . This step is the one described in the Appendix. In a second step the second equation is solved using Γ_u as excitation and now Γ_t and Γ_d are calculated. The first equation is solved again with all terms and so on. At every step a single interface is considered and only two vectors of coefficients (\mathbf{R} , \mathbf{U}^0) or (\mathbf{D}^0 , \mathbf{T}) have to be determined, which makes the solving easier by matrix inversion. Furthermore the relative contributions of successive scattering orders can be more easily identified if needed. The iterative process is continued until all coefficients are converged, which is typically achieved in four iterations.

3.2. Implementation of the Kutta condition

The aforementioned procedure would be the same in a medium at rest and requires introducing the effect of the vane wakes for physical consistency. Indeed in the presence of a mean flow, the fluctuating motion has to comply with the Kutta condition that imposes zero pressure jump at the trailing edges of the vanes. This condition significantly redefines the strengths of the scattered waves produced by the mode-matching technique, especially as the mean-flow Mach number increases, as pointed out by Bouley et al. [44]. In the mode-matching procedure the zero pressure jump between both sides of a vane must be enforced just upstream of the trailing edges inside the inter-vane channels, which is equivalent to a new constraint on the modes. An additional equation involving the vectors of modal amplitudes in the reference channel is written as

$$\sum_{m=0}^{\infty} (K - K_m^- M) [1 - (-1)^m e^{-iu}] U_m^0 = - \sum_{m=0}^{\infty} e^{iK_m^+ c/\beta} [1 - (-1)^m e^{-iu}] (K - K_m^+ M) D_m^0. \quad (14)$$

Without any further modification this would end up with an over-determined linear system. But the Kutta condition results in the continuous shedding of vorticity in the wake. This is accounted for by distributing lines of concentrated vorticity in the continuation of the vanes. The strength of the vorticity vector in the direction normal to the unwrapped plane is expressed in the sense of generalized functions and reads

$$\Omega_K(x, y) = \Omega_0 e^{iKx/M_0} \sum_{\nu=-\infty}^{+\infty} e^{i\nu y} \delta(y - \nu h), \quad X \geq c/\beta \quad (15)$$

where Ω_0 is a magnitude factor introduced as a new unknown. This vortical field is also expanded as a series of oblique gusts, in the form

$$\Omega_K(x, y) = \frac{\Omega_0}{h} \sum_{q=-\infty}^{+\infty} b_q e^{iKx/M_0} e^{i\alpha_q y}, \quad X \geq c/\beta. \quad (16)$$

The associated velocity field \mathbf{v}_K^h is obtained from the definition of the vorticity $\Omega_K = \nabla \times \mathbf{v}_K^h$ and from its incompressibility ($\nabla \cdot \mathbf{v}_K^h = 0$). The expression of the axial velocity becomes

$$v_{x,K}^h(x, y) = \sum_{q=-\infty}^{+\infty} \frac{i\Omega_0 \alpha_q}{h(\alpha_q^2 + (K/M_0)^2)} e^{iKx/M_0} e^{i\alpha_q y}. \quad (17)$$

This hydrodynamic contribution is included in the matching equation for the axial velocity at the trailing-edge interface as an additional term in the Γ vector of Eq. (11). Because the hydrodynamic field is pressure-free, the matching equation for the pressure remains unchanged when the Kutta condition is imposed.

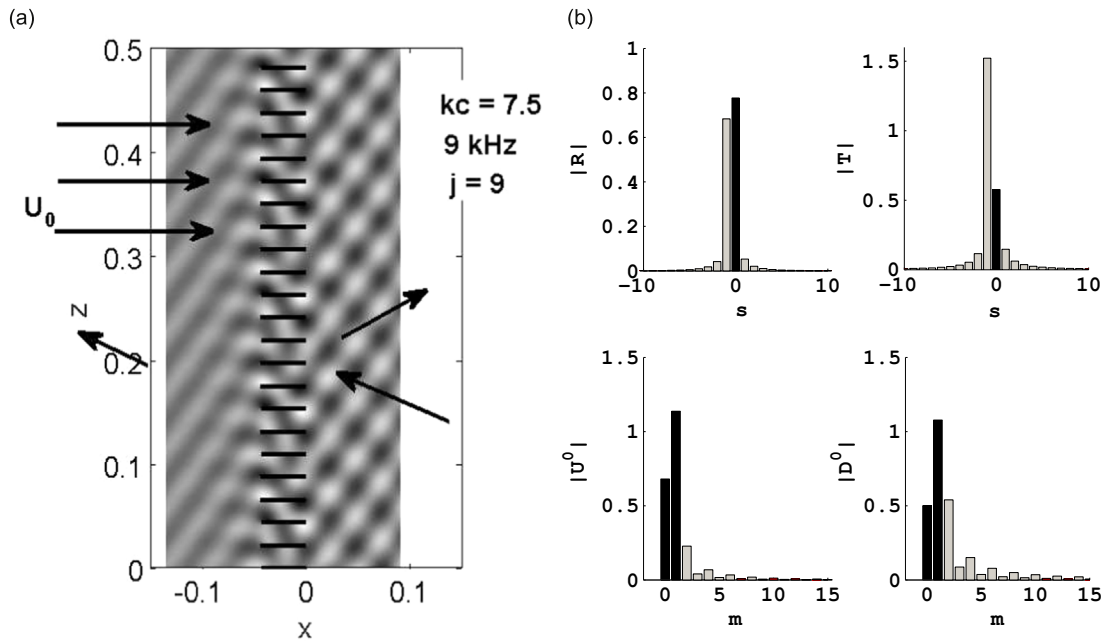


Fig. 5. Scattering of the incident plane-wave mode $j=9$. (a) Instantaneous sound pressure pattern. (b) Modal coefficients, *grey* for cut-off and *black* for cut-on. $M_0 = 0.15$, $V=23$, frequency: 9 kHz.

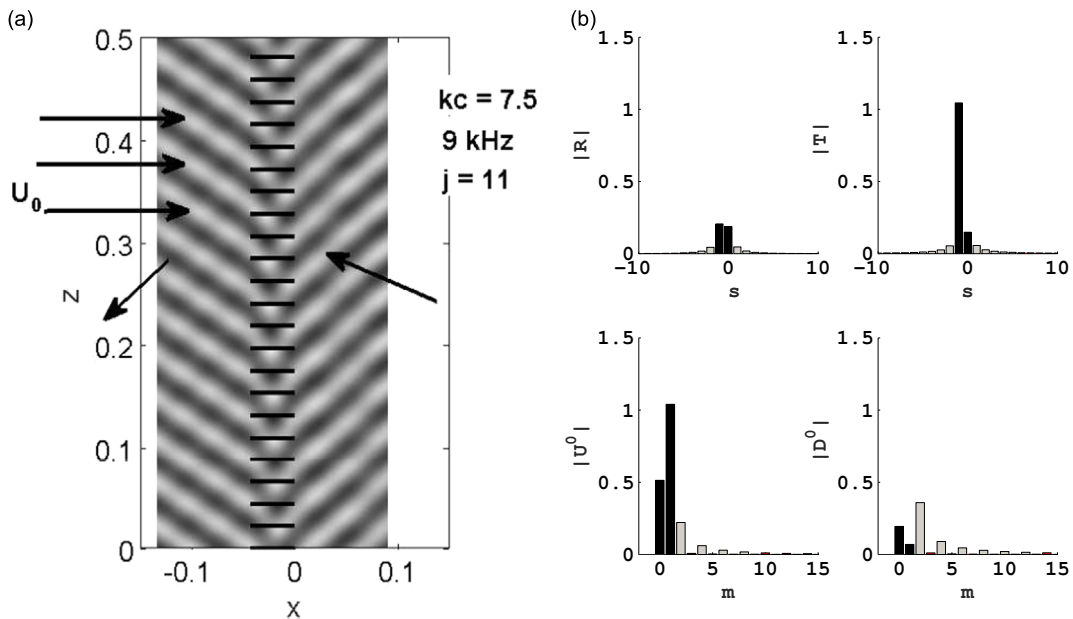


Fig. 6. Scattering of the incident plane-wave mode $j=11$. (a) Instantaneous sound pressure pattern. (b) Modal coefficients, *grey* for cut-off and *black* for cut-on. $M_0 = 0.15$, $V=23$, frequency: 9 kHz.

3.3. Scattering of elementary waves

Prior to full computations of edge-dipole scattering, inspecting the response of the cascade to elementary incident plane-wave modes from downstream allows highlighting fundamental properties of the cascade. This is achieved in this section for the unwrapped model stator shown in Fig. 2, with a number of flat-plate vanes $V=23$ and an axial-flow Mach number of 0.15. The reference radius is $r_c=0.08$ m. The selected frequency is 9 kHz, corresponding to Helmholtz numbers based on the channel height and on the vane chord of 3.6 and 7.5, respectively. At this frequency the channel modes of orders $m=0$ and $m=1$ are cut-on but higher-order modes are cut-off. This set of parameters typically corresponds to the small-size fans used

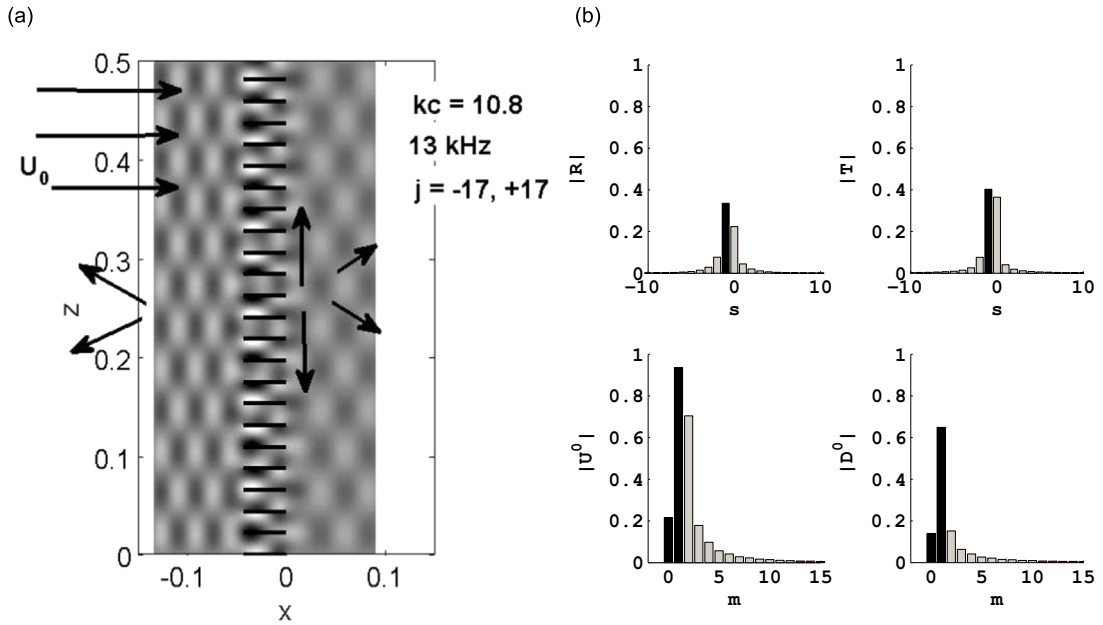


Fig. 7. Scattering of the combined incident modes $j=17$ and $j=-17$ with source at the trailing-edge interface. (a) Instantaneous sound pressure pattern. (b) Modal coefficients for $j=17$, (grey) for cut-off and (black) for cut-on. $M_0 = 0.15$, $V=23$, frequency: 9 kHz.

in air-conditioning systems for aircraft. The results for the incident plane-wave modes $j=9$ and $j=11$ are investigated first and reported in Figs. 5 and 6. The left-side part of each figure shows an instantaneous pressure wavefront pattern and the right-side part displays the amplitudes of all modal coefficients as bar-graphs. Conventionally the incident mode has an upward phase speed.

The mode $j=9$ (Fig. 5) is scattered into the modes $n = 9 \pm 23s$ both in the reflection and in the transmission, so that the lowest generated order except $n=9$ is $n = -14$, noting that this mode is the first cut-off one in the present conditions. Therefore the upstream-transmitted wave is made of the mode 9 (or $s=0$) only. The field (Fig. 5a) is typical of the vicinity of the transition between a low-frequency regime for which only one mode is cut-on and a high-frequency regime for which two modes are cut-on away from the cascade. The reflection is quite strong and the field in the upstream vicinity of the cascade clearly exhibits an evanescent part. The example of the mode $j=11$ (Fig. 6) is featuring a clear transfer from the incident mode into another dominant mode in the upstream transmission, with inversion of the phase-speed direction. Indeed the scattered modes $n = 11$ and $n = -12$ are both cut-on but the latter ($s=1$) is of much larger amplitude than the former ($s=0$) in the upstream domain, as indicated by the diagram in Fig. 6b. Reminding that the cascade is an unwrapped representation of a stator, this means that the dominant component of the transmitted wave is spinning in the opposite direction with respect to the incident wave. Still different behaviors could be described for other modes, not detailed here.

Because the excitation of the trailing-edge interface is produced by dipoles at a vanishing distance from the edges in the present model, even the evanescent components of the oblique-wave expansion of Section 2.2 contribute to the radiated field, as a result of modal scattering. But the same analysis as above in terms of isolated incident plane-wave modes for evanescent waves would be misleading because they would increase exponentially away from the cascade downstream. Such excitation modes need to be analyzed by combining the opposite of the component of index $-j$ with the component of index j . Furthermore the downstream part of the excitation must be removed and replaced by the complementary downstream-emitted decaying wave. Such a test is reported in Fig. 7 for the doublet of modes ($j = -17, j = +17$), again at the frequency of 9 kHz. Looking for the periodicity 17, the plot does not exhibit any radiating pattern but only a trace localized in the very vicinity of the vanes. Yet the scattering produces all modes of orders $n = \pm 17 - 23s$ and in particular the modes $n = +6$ and -6 ($s = \pm 1$) that are cut-on at this frequency. This is why the latter modes contribute to the radiated field both upstream and downstream. For this reason a substantial number of cut-off modes must be included in the plane-wave expansion of the series of edge dipoles according to Eq. (5).

4. Stator broadband noise formulation

4.1. Scattered field of an edge dipole

The complete response of the cascade for an edge-dipole at a single vane is determined by summing all plane-wave mode contributions according to Eq. (5). An *a priori* questionable point is that the coefficients \bar{a}_j of the pressure waves do

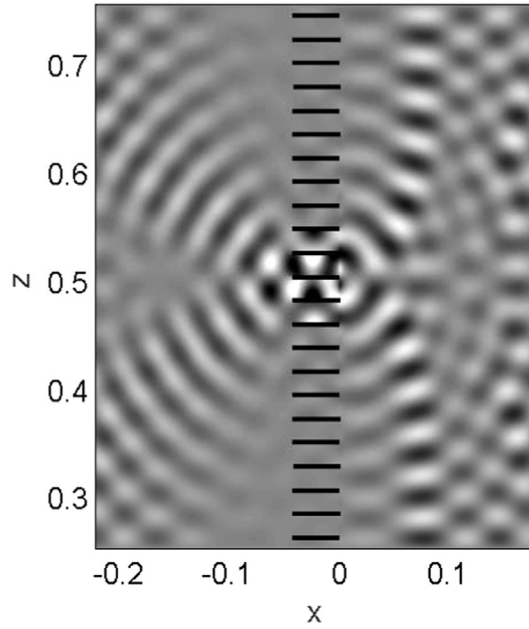


Fig. 8. Instantaneous sound pressure pattern for the diffraction of a single edge-dipole at the center vane ($\epsilon = 0$). Flow from left to right, $M_0 = 0.15$, $V = 23$, frequency: 9 kHz.

not tend to zero for arbitrarily increasing values of j (see Eq. (7)). This is not prejudicial when synthesizing the direct pressure field in Fig. 4 since large values of j correspond to evanescent waves with increasing damping rates. These waves cannot be seen away from the interface. But incident modes of large orders contribute when calculating the response of the stator because of the modal scattering. This is why a small but finite distance ϵ of the edge dipole to the trailing edge has been introduced and tested, the effect of which is to multiply the expression of \bar{a}_j by the factor $e^{iKM_0\epsilon} e^{ij\pi\epsilon/(\bar{a}_j(Vh)^2)}$. The small parameter ϵ must be such that $k\epsilon \ll 1$ to ensure a proper tuning of the edge dipole by invoking the asymptotic behavior of the half-plane Green's function. Indeed the latter produces a strong amplification of the radiated field of the dipole with the factor $(k\epsilon)^{-1/2}$ [36]. In contrast the coefficients a_j of the potential waves involved in the calculation of the acoustic powers of the scattered waves do vanish for large values of j . It has been found that the results are not sensitive to the value of ϵ as long as it remains small (much less than one percent of chord in the present case), proving the robustness of the proposed approach.

A typical result combining all modes of orders j between -20 and 20 is plotted in Fig. 8 in terms of instantaneous pressure, again for the same frequency of 9 kHz. As shown in Section 2.2, 20 incident modes are sufficient to reproduce the dipole excitation. The trailing-edge dipole is located on the center vane in order to emphasize the scattering by neighboring vanes. The two directly excited channels as well as the next two adjacent ones respond dominantly, whereas the pressure field is of much lower amplitude in more distant channels. As a result the upstream field exhibits two main oblique lobes that are fed by the four most excited channels, with secondary interference fringes. The obliqueness corresponds to spinning patterns in the annular space. The field downstream is substantially different because the dominant direction of radiation of the edge-dipole is tangent to the trailing-edge interface.

4.2. Predicted power spectra

The same two-dimensional approach is now applied to illustrate the feasibility of trailing-edge broadband noise predictions using the mode-matching technique, provided that the strength of the edge dipole is determined. For this some similarity is recognized with Amiet's model of isolated-airfoil trailing-edge noise, according to which the far-field sound is related to the statistical properties of the hydrodynamic wall-pressure field closely upstream of the trailing edge. More precisely the far-field sound intensity is found proportional to the product $L\Phi_{pp}(\omega)\ell_y(\omega)$ where L is the spanwise extent, $\Phi_{pp}(\omega)$ is the hydrodynamic wall-pressure spectrum and $\ell_y(\omega)$ the associated spanwise correlation length near the trailing edge [38]. The same holds for the in-duct power at any frequency and the classical definition of the axial acoustic intensity in a uniform base flow [45] is used to compute the acoustic power. For a potential of generic expression

$$\phi = \sum_{j=-\infty}^{\infty} C_j e^{ij2\pi y/(Vh)} e^{-i(\pm K^{(j)} + M_0 K)X}$$

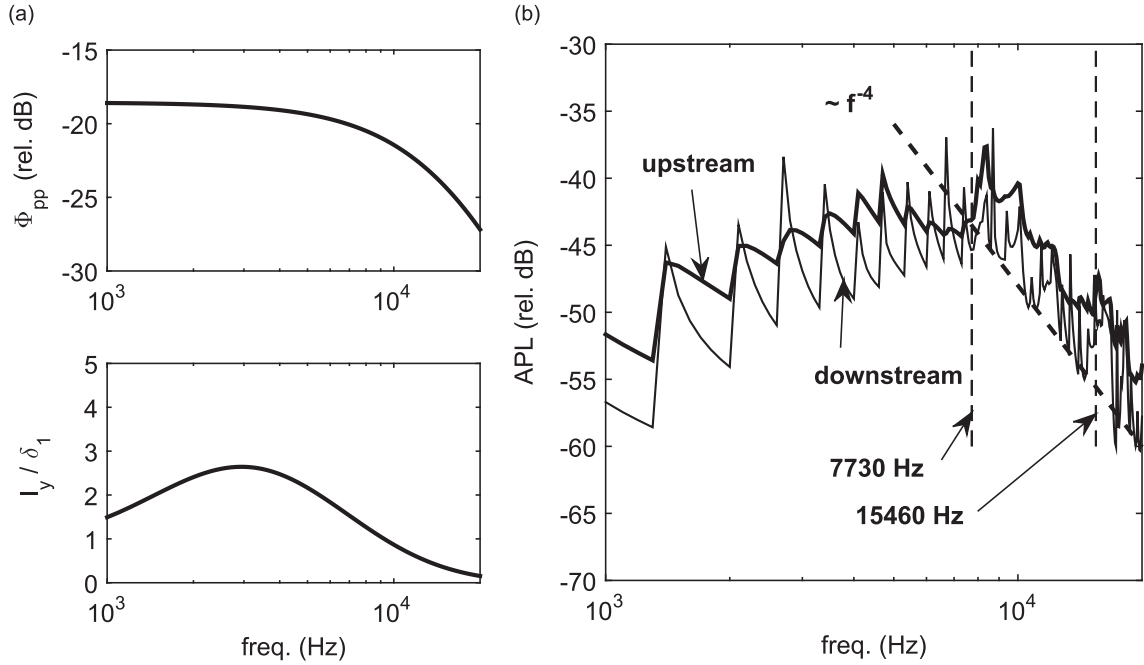


Fig. 9. (a) Test-case wall-pressure statistical data: spectrum in dB/Hz, spanwise correlation length scaled by the displacement thickness. (b) Downstream and upstream power spectra (per unit span and per vane). All plane-wave modes up to $|j|=100$. Cut-off frequencies of the first two channel modes indicated as dashed lines.

away from the cascade the expression of the intensity reads

$$I = \mp k\beta^2 \rho_0 c_0 \sum_{j=-\infty}^{\infty} |C_j|^2 \text{Re}\{K^{(j)}\}$$

where the + and the – signs correspond to downstream and upstream propagation, respectively. The real part of the axial wavenumbers in the expression highlights that only the cut-on modes carry acoustic energy. The intensity is uniformly distributed over the duct cross-section and the power is simply obtained by multiplying by the cross-section area. The latter is $2\pi R_0 L$ with $L = R_2 - R_1$ in the unwrapped cascade representation. In the present test case the hub and tip radii are not specified. Furthermore the two-dimensional reduction is equivalent to assume homogeneously distributed sources along the span. Calculations are only aimed at providing values for the acoustic power per unit span. In other words the squared amplitude of the edge dipole is proportional to the product $\Phi_{pp}(\omega)\ell_y(\omega)$. Furthermore trailing-edge noise is not vane-to-vane correlated, so that the total acoustic power is the power from one vane multiplied by the number of vanes.

Both Φ_{pp} and ℓ_y are now required as input data. When they are unknown, empirical expressions proposed by many authors can be used, in terms of either outer or inner boundary-layer variables, accounting or not for the adverse pressure gradients characteristic of loaded airfoils (for a review see [46]). The present test is addressing a family of fans rather than a precise real fan; as such it cannot produce true quantitative results. Therefore only relative decibel levels are targeted, with emphasis on the intrinsic efficiency with which the cascade radiates upstream and downstream as a function of frequency. A corrected form of the expression proposed by Gliebe et al. [47] for $\Phi_{pp}(\omega)$ and an empirical fit tuned on data reported by Guédél et al. [48] for $\ell_y(\omega)$ are retained here for simplicity, essentially because they only require an estimate of the displacement thickness δ_1 as a minimum information. The corresponding formulae read

$$\Psi_{pp}(\omega) = \frac{\Phi_{pp}(\omega)}{\rho_0^2 \delta_1 U_0^3} = \frac{10^{-4}}{(1 + 0.3\bar{\omega}^2)^{5/2}}, \quad \frac{\ell_y(\omega)}{\delta_1} = e^{-2\bar{\omega}} + \frac{a}{\sqrt{2\pi\sigma\bar{\omega}}} e^{-(\ln\bar{\omega} - \ln 0.44)^2 / (4\sigma^2)},$$

introducing the dimensionless frequency $\bar{\omega} = \omega\delta_1/U_0$, with $\sigma = 0.55$, $a = 1.5$. The quantities Ψ_{pp} and $\ell_y(\omega)/\delta_1$ are plotted in Fig. 9a. The wall-pressure spectrum drops beyond 10 kHz with the classical high-frequency roll-off $\bar{\omega}^{-5}$. The maximum correlation length is reached around 3 kHz and decreases very fast at higher frequencies. Both trends combine as a counterpart to the increased radiation efficiency resulting from higher modal content at high frequencies.

It must be kept in mind that only the cut-on modes contribute to the power transmitted through the duct but that such modes can be generated by cut-off modes of the expansion in Section 2.2. The cut-off frequency of the first oblique wave in the unwrapped perimeter $2\pi r_c$ is 676 Hz for the mean radius r_c of 80 mm in the present test case. Therefore no trailing-edge noise can be predicted below this frequency because the edge dipole is oriented normal to the duct axis and cannot excite the axial plane-wave known to be always cut-on (the absence of any contribution from this wave can be recognized in Fig. 8). This

limitation is inherent to the zero-stagger simplification. For staggered outlet guide vanes modeled by inclined flat plates the edge dipole would be inclined accordingly and would also excite the axial plane-wave mode. The limitation is not a serious issue because trailing-edge noise sources are weak at low frequencies, for which other sources would dominate in a real turbomachinery stage. In addition, the scattered axial plane wave is not expected in the present application for two reasons. First, the incident axial plane-wave mode has a zero magnitude because of the dipolar nature of the excitation. Secondly, only the incident waves of azimuthal orders that are multiples of the number of vanes ($V=23$) can generate scattered axial plane waves. For these large azimuthal orders (above 20 or 100), the amplitude of the excitation is expected to be negligible, so is the associated acoustic response. Furthermore the excitation of the axial plane wave is expected more upstream than downstream where the vanes are actually aligned with the axis. Accounting for different stagger angles at the trailing edge and at the leading edge is a possible extension of the iterative mode-matching procedure not addressed in the present work. This could be achieved by coupling the model of sound propagation through bent ducts of slowly varying cross-section developed by Brambley and Peake [49] and Whitehead's theory of staggered waveguides [26]. In the present investigation the axial plane wave is considered to negligibly contribute in the middle and high frequency range of major interest.

Predicted power spectra in a relative decibel scale, again for the same cascade configuration, are shown in Fig. 9b. Repeated calculations with different number of modes did not produce any difference, which indicated that the convergence is reached. The plotted quantity is the power per unit span, radiated either downstream or upstream. The wall-pressure statistics is only used here to reproduce a realistic spectral envelope over the range 1–20 kHz, even though considering a spanwise correlation length within the scope of a two-dimensional theory is questionable. The chord length is 45 mm and the displacement thickness at the trailing-edge is arbitrarily taken as 0.8 mm (typical of significantly loaded vanes). In practice it would depend on the vane design and on the operating point of the considered fan. The axial flow speed is of 50 m/s. The radiated power first increases with frequency and then decreases, as a result of the combined increasing acoustic efficiency and high-frequency energy drop in the involved hydrodynamic excitation. The cut-off frequencies of the first two transverse modes in the inter-vane channels of height 22 mm are 7730 Hz and 15460 Hz; they are indicated in Fig. 9b as vertical dashed lines. As expected from the analytical expression of the axial wavenumbers \bar{a}_j , Eq. (7), peak responses are found at cut-off frequencies of the plane-wave modes away from the cascade. The peaks are especially marked downstream. It is guessed that these resonances are artificially emphasized by the two-dimensional model and its geometrical simplifications. As a result the dips of the spectral shape are more representative than the peaks, so that giving more confidence to the former probably provides a better estimate of the true sound. Finally the overall power level is predicted higher upstream than downstream by about 3 dB. This imbalance is somewhat expected from the asymptotic cardioid radiation pattern of the trailing-edge noise of isolated airfoils at high frequencies. Yet it could be questioned by cascade scattering. Furthermore considering staggered vanes would possibly redistribute the energy differently in the upstream and downstream directions because of the inclination of both the edge dipoles and the vanes. Indeed different trends are reported in the literature, based on experimental studies. For instance in the Boeing 18-in Fan test rig, Ganz et al. [50] report broadband noise spectra for the rotor alone where the inlet radiation is lower than the aft radiation. Glegg showed that the difference can be up to 10 dB between 10 kHz and 20 kHz at low loading and a small tip gap of 0.02 in [51]. Yet as shown in Ganz et al. [50] or Rozenberg [52], this difference can be much lower at other loading conditions and tip clearance. Similarly, Woodward et al. [53] showed in the fan noise Source Diagnostic Test (SDT) case that the forward-radiated noise was slightly larger than the aft-radiated one. In all these cases, the rotors had significantly staggered blades, and the experimental results were available for the rotor self-noise only. If the latter was assumed to be essentially trailing-edge noise nearly the same power would be expected upstream and downstream in view of the present investigation because the blades would be almost perpendicular to the axis. Finally the present results remain compatible with existing databases.

With the present input data the acoustic power spectrum exhibits an overall high-frequency decrease with the power (-4) of the frequency, emphasized by the dashed oblique line in Fig. 9b. This trend must be understood as only indicative; it could differ with other wall-pressure statistics.

It is worth noting that the present two-dimensional model could be used to estimate the trailing-edge noise of a real stator from some knowledge of the boundary-layer displacement thickness at the vane trailing edges, ignoring all other detailed flow features, which is of large engineering interest. Nevertheless the methodology is only relevant for large numbers of outlet guide vanes and large hub-to-tip ratios. In more general configurations an approach currently used in the literature consists in splitting the annular cascade into a series of strips and unwrapping each strip to describe it as a two-dimensional cascade. Even if the radial extent of each annulus is defined in such a way that adjacent annuli are not correlated such an approach neglects the scattering of sources located at a radius by the walls at other radii. This is why the present formulation is only considered as a preliminary step. The mode-matching procedure can be easily transposed to a true annular cascade in cylindrical coordinates, precisely taking benefit from the fact that the spanwise correlation length of the sources is generally much smaller than the duct height. Edge dipoles could still be defined and distributed along the trailing edges with their individual direct fields expanded in a series of modes, referring to Green's function of the annular duct [45]. The scattering of each mode by the full annular cascade could be determined exactly as long as the inter-vane channels can be considered as three-dimensional bifurcated waveguides with radial walls. Such an extension is presently in progress [54]. It will have the advantages of running without any splitting in strips and of avoiding the artificial parallelism of adjacent vane walls.

5. Conclusion

The new formulation proposed in this study provides a simple way of solving the trailing-edge noise problem for a row of outlet guide vanes in an axial turbomachine. The vanes are considered as a rectilinear cascade of zero-stagger plates in an unwrapped two-dimensional representation ensuring the periodicity of the stator. The first key step is the definition of a so-called edge dipole that is shown to be equivalent to the trailing-edge noise sources of a single vane at a given frequency. This dipole is approached at a vanishing distance to the edge from downstream. Its direct field is expanded into a series of plane-wave modes. In a second step the diffraction of each mode by the cascade is calculated considering the cascade as a periodic array of bifurcated waveguides and using a mode-matching technique. For this the mean flow is assumed uniform and a full Kutta condition is applied at the trailing edges. The total field of the dipole is obtained by summing all diffracted fields of the aforementioned plane-wave modes. It is also expressed as a series of modes, amongst which only the cut-on modes carry energy away from the cascade. The total acoustic power emitted by the stator is simply the power from one vane multiplied by the number of vanes. The finite chord length of the stator is a parameter of the model and the formulation holds for any arbitrary subsonic Mach number and frequency.

A first evaluation of the newly developed model taking empirical wall-pressure statistics available in the literature as input data has been made in a configuration of small-scale and low-speed axial fan. The results show that upstream radiation is typically 3 dB higher than downstream radiation, which has been experimentally observed previously. The practical calibration of the amplitude of the edge dipole is made by comparing the wall-pressure distributions produced by Amiet's model and by the half-plane Green's function for a lift dipole close to the edge, which implies that the actual distance of the dipole to the edge is an important parameter entering the model. Moreover this distance is not uniquely defined: the shorter it is, the smaller the amplitude of the edge dipole is. It has been verified that the sound power predictions do not significantly change if the edge dipoles are located at some finite distance ε instead of exactly at the trailing-edge interface, as long as the Helmholtz number $k\varepsilon$ remains much smaller than 1. This ensures the robustness of the model. Instantaneous acoustic pressure contours also stress the significant diffraction cascade effect which has not been accounted for previously. Yet the present estimates neglect the stagger angle of the vanes at the leading edge. Including this parameter in the analysis is identified as a first necessary extension.

The main advantages of the mode-matching technique are its formal simplicity and exactness in the considered geometry. It has large possibilities of extension that motivated the present effort. The two-dimensional extension to the case of staggered flat-plates is straightforward as long as adjacent vanes significantly overlap. The method can also be generalized in a three-dimensional context to address annular cascades of vanes in cylindrical coordinates without any need to resort to a strip theory, at least for unswept and untwisted vanes, which is a reasonable simplification in many designs. Finally, it is worth noting that channel modes or duct modes can also be defined for absorbing walls by replacing the present underlying rigid-wall boundary condition by an impedance condition, which makes the mode-matching technique even more attractive.

Acknowledgments

The present developments have been partially made in the EC-funded project ACP2-GA-2012-314066 IDEALVENT (Integrated Design of Optimal Ventilation Systems for Low Cabin and Ramp Noise) and partially in the industrial chair ADOPSYS supported by SNECMA and the French Agency ANR.

Appendix A. Mode-matching procedure

The mode-matching procedure dedicated to sound-generation and sound-transmission problems has been thoroughly detailed by Bouley et al. [44]. Only the main steps are reproduced here for the sake of completeness. The main idea is that the cascade of vanes and its vicinity are considered as multiple sub-domains of space in which the same convected Helmholtz equation holds. This implicitly imposes that the uniform flow considered in the analysis is parallel to the walls. The domains of interest are the upstream and downstream regions and the inter-vane channels understood as a periodic array of bifurcated waveguides. The various sub-domains communicate by the leading-edge and trailing-edge interfaces. In each sub-domain the solution for the acoustic field can be expressed as a series of modes the form of which is imposed by lateral boundary conditions. The latter are a rigid-wall condition for the channels and a periodicity condition in the upstream and downstream regions. The modes differ from one subdomain to another one but the acoustic field must be continuous. The continuity is ensured by writing some matching conditions at the interface. In turbomachinery gas dynamics, the quantities to be conserved are the mass flow rate and either the total enthalpy for a row of stationary vanes or the rothalpy for a rotating blade row. The associated equations are linearized when addressing small oscillatory motions. In the present case the general conservation laws reduce to the continuity of the fluctuating pressure and axial velocity at the interfaces [55]. The same conditions are classically applied for sound transmission problems in bifurcated waveguides in the absence of flow.

The problem of the primary scattering of an upstream-propagating oblique plane wave by the trailing-edge interface is formulated in this appendix for semi-infinite vanes and ignoring the Kutta condition, as a preliminary step. The incident wave of azimuthal index j forces transmitted cosine modes in the channels, of amplitudes A_m^j and shape functions $\cos(m\pi y/h)$, that propagate upstream, with a phase shift between adjacent channels imposed by the angle of incidence. A series of reflected, downstream-propagating waves of coefficients B_s^j and transverse phases $e^{i\alpha_s^j y}$ with $\alpha_s^j = (j+sV)2\pi/(Vh)$ are also generated because the transverse periodicity of the incident wave is modulated by the periodicity of the cascade. All waves are matched at the interface by imposing the continuity conditions. An infinite linear system of equations is obtained, solved by matrix inversion after being reduced by modal projection.

The acoustic potential ϕ is used as the primary variable from which the pressure and velocity are deduced as (for the convention $e^{-i\omega t}$)

$$p = i\rho_0\omega\phi - \rho_0U_0\frac{\partial\phi}{\partial x}, \quad v_x = \frac{\partial\phi}{\partial x}.$$

In view of the expression of the acoustic pressure derived in Section 2.2 the incident plane wave of index j from downstream has the potential

$$\phi_i = a_j e^{ij2\pi y/(Vh)} e^{-i(K^{(j)} + M_0K)x}$$

with

$$\bar{a}_j = ia_j \frac{\rho_0 c_0}{\beta} (K + M_0K^{(j)}) \quad K^{(j)} = \sqrt{K^2 - \left(\frac{j2\pi}{Vh}\right)^2}$$

The transmitted potentials in the inter-vane channels are expressed as sums of cosine modes. Now adjacent inter-vane channels have phase-shifted responses driven by the obliqueness of the incident wave, in such a way that the coefficients in the channel of index ν are those of the reference channel ($\nu = 0$) multiplied by $e^{i\nu u}$ with $u = j2\pi/V$. As a result the transmission problem only needs to be solved for the reference channel, in which the transmitted potential reads

$$\phi_t = \sum_{m=0}^{\infty} A_m^j \cos\left(\frac{m\pi y}{h}\right) e^{-i(K_m + M_0K)x} \quad \text{with } K_m = \sqrt{K^2 - \left(\frac{m\pi}{h}\right)^2}.$$

Finally the reflected field is a sum of oblique plane waves written as

$$\phi_r = \sum_{s=-\infty}^{\infty} B_s^j e^{i\alpha_s^j y} e^{i(\bar{K}_s^j - M_0K)x} \quad \text{with } \bar{K}_s^j = \sqrt{K^2 - \alpha_s^{j2}}; \quad \alpha_s^j = (j+sV)\frac{2\pi}{Vh}.$$

If the trailing-edge interface is placed at $x=0$ in a first step the matching equations read

$$\sum_{m=0}^{\infty} A_m^j \cos\left(\frac{m\pi y}{h}\right) = a_j e^{ij2\pi y/(Vh)} + \sum_{s=-\infty}^{\infty} B_s^j e^{i\alpha_s^j y}, \tag{A.1}$$

$$\sum_{m=0}^{\infty} (K_m + M_0K) A_m^j \cos\left(\frac{m\pi y}{h}\right) = a_j (K^{(j)} + M_0K) e^{ij2\pi y/(Vh)} - \sum_{s=-\infty}^{\infty} B_s^j (\bar{K}_s^j - M_0K) e^{i\alpha_s^j y}. \tag{A.2}$$

These equations are first reduced by projection on the modes of the inter-vane channels, considering only the reference channel $0 \leq y \leq h$ and the integrals

$$I_m^j = \int_0^h e^{ij2\pi y/(Vh)} \cos\left(\frac{m\pi y}{h}\right) dy, \quad J_m^{s,j} = \int_0^h e^{i\alpha_s^j y} \cos\left(\frac{m\pi y}{h}\right) dy,$$

keeping in mind that j cannot be zero in the present case. The following expressions are found for I_m^j :

$$I_m^j = \frac{j2\pi}{Vh} \frac{[1 - (-1)^m e^{i2\pi j/V}]}{\left(\frac{2\pi j}{Vh}\right)^2 - \left(\frac{m\pi}{h}\right)^2} \quad \text{if } m \neq \pm \frac{2j}{V},$$

$$I_m^j = \frac{h}{2} \quad \text{if } m = \pm \frac{2j}{V},$$

and similar ones are obtained for $J_m^{s,j}$ when replacing $j2\pi/(Vh)$ by α_s^j , with the value $h\delta_{0,m}$ if $j+sV = 0$.

Eqs. (A.1) and (A.2) lead to

$$A_m^j \frac{h}{2} (1 + \delta_{0,m}) = a_j I_m^j + \sum_{s=-\infty}^{\infty} B_s^j J_m^{s,j}, \tag{A.3}$$

$$(K_m + M_0K) A_m^j \frac{h}{2} (1 + \delta_{0,m}) = a_j (K^{(j)} + M_0K) I_m^j - \sum_{s=-\infty}^{\infty} B_s^j (\bar{K}_s^j - M_0K) J_m^{s,j}. \tag{A.4}$$

Now the trailing-edge interface is also the source of the excitation in the present problem. Therefore, after the matching equations (A.3) and (A.2) are solved, the total field downstream of the interface must be cleaned of the incident plane wave and added to the complementary downstream-travelling component of the expansion illustrated in Fig. 4.

It is worth noting that the mode-matching procedure as described above can be applied in the same way to formulate the scattering of a downstream-propagating oblique wave at the leading-edge interface of a stator, by simply changing the sign of the Mach number. Yet in the present case a Kutta condition must be imposed at the trailing edges of the vanes. This condition is equivalent to force the pressure jump between both sides of a vane to go to zero when approaching the trailing-edge from upstream and adding thin vorticity sheets downstream of the trailing edges (Section 3.2).

References

- [1] J.E. Ffowcs-Williams, D.L. Hawkins, Theory relating to the noise of rotating machinery, *Journal of Sound and Vibration* 10 (1) (1969) 10–21.
- [2] R. Mani, G. Horvay, Sound transmission through blade rows, *Journal of Sound and Vibration* 12 (1) (1970) 59–83.
- [3] S. Kaji, T. Okazaki, Generation of sound by rotor–stator interaction, *Journal of Sound and Vibration* 13 (1970) 281–307.
- [4] S. Kaji, T. Okazaki, Propagation of sound waves through a blade row, I. Analysis based on the semi-actuator disk theory, *Journal of Sound and Vibration* 11 (3) (1970) 339–353.
- [5] S. Kaji, T. Okazaki, Propagation of sound waves through a blade row, II. Analysis based on the acceleration potential method, *Journal of Sound and Vibration* 11 (3) (1970) 355–375.
- [6] W. Koch, On transmission of sound through a blade row, *Journal of Sound and Vibration* 18 (1) (1971) 111–128.
- [7] R.K. Amiet, Transmission and reflection of sound by two blade rows, *Journal of Sound and Vibration* 34 (3) (1974) 399–412.
- [8] M. Namba, Three-dimensional analysis of blade force and sound generation for an annular cascade in distorted flows, *Journal of Sound and Vibration* 50 (1977) 479–508.
- [9] W. Koch, Sound generation and blade vibrations of cascaded flat plates in subsonic flow, *Improvements in Turbomachines and Related Techniques* (1981) 51–99.
- [10] C.S. Ventres, M.A. Theobald, W.D. Mark, Turbofan Noise Generation, Volume 1: Analysis, Contractor Report CR-167952, NASA, 1982.
- [11] D.S. Whitehead, An actuator disc analysis of unsteady subsonic cascade flow, *Journal of Sound and Vibration* 109 (2) (1986) 207–213.
- [12] N. Peake, The interaction between a high-frequency gust and a blade row, *Journal of Fluid Mechanics* 241 (1992) 261–289.
- [13] S.J. Majumdar, N. Peake, Three-dimensional effects in cascade–gust interaction, *Wave Motion* 23 (1996) 321–337.
- [14] J.M.R. Graham, The effect of a two-dimensional cascade of thin streamwise plates on homogeneous turbulence, *Journal of Fluid Mechanics* 356 (1998) 125–147.
- [15] S.A.L. Glegg, The response of a swept blade row to a three-dimensional gust, *Journal of Sound and Vibration* 227 (1) (1999) 29–64.
- [16] B. Elhaddidi, H.M. Atassi, High frequency sound radiation from an annular cascade in swirling flows, *8th AIAA/CEAS Aeroacoustics Conference and Exhibit*, Breckenridge, Colorado, AIAA Paper 2002-2560, 2002, pp. 1–11.
- [17] I. Evers, N. Peake, On sound generation by the interaction between turbulence and a cascade of airfoils with non-uniform mean flow, *Journal of Fluid Mechanics* 463 (2002) 25–52.
- [18] O. Boquillon, S.A.L. Glegg, W.J. Devenport, J. Larsan, The interaction of large scale turbulence with a cascade of flat plates, *9th AIAA/CEAS Aeroacoustics Conference and Exhibit*, Hilton Head, South Carolina, AIAA Paper 2003-3289, 2003, pp. 1–8.
- [19] S. Job, E. Lunville, J.F. Mercier, Diffraction of an acoustic wave by a plate in a uniform flow: a numerical approach, *Journal of Computational Acoustics* 13 (November) (2004) 1–21.
- [20] A.J. Cooper, N. Peake, Upstream-radiated rotor–stator interaction noise in mean swirling flow, *Journal of Fluid Mechanics* 523 (2005) 219–250.
- [21] M. Nallasamy, E. Envia, Computation of rotor wake turbulence noise, *Journal of Sound and Vibration* 282 (2005) 649–678.
- [22] C. Cheong, P. Joseph, L. Soogab, High-frequency formulation for the acoustic power spectrum due to cascade–turbulence interaction, *Journal of the Acoustical Society of America* 119 (January (1)) (2006) 108–122.
- [23] H. Posson, M. Roger, S. Moreau, Upon a uniformly valid analytical rectilinear cascade response function, *Journal of Fluid Mechanics* 663 (2010) 22–52.
- [24] S.M. Grace, Fan broadband interaction noise modeling using a low-order method, *Journal of Sound and Vibration* 346 (2015) 402–423.
- [25] S.A.L. Glegg, C. Jochault, Broadband self-noise from a ducted fan, *AIAA Journal* 36 (August (8)) (1998) 1387–1395.
- [26] E.A.N. Whitehead, The theory of parallel-plate media for microwave lenses, *Proceedings of the IEE-Part III: Radio and Communication Engineering* 98 (52) (1951) 133–140.
- [27] M. Roger, B. François, S. Moreau, Towards cascade trailing-edge noise modeling using a mode-matching technique, *21th AIAA/CEAS Aeroacoustics Conference*, AIAA Paper 2015-2541, Dallas, TX, 2015.
- [28] M.S. Howe, A review of the theory of trailing edge noise, *Journal of Sound and Vibration* 61 (3) (1978) 437–465.
- [29] J.E. Ffowcs-Williams, L.H. Hall, Aerodynamic sound generation by turbulent flow in the vicinity of a scattering half-plane, *Journal of Fluid Mechanics* 40 (1970) 657–670.
- [30] R.K. Amiet, Noise due to turbulent flow past a trailing edge, *Journal of Sound and Vibration* 47 (3) (1976) 387–393.
- [31] J.E. Ffowcs-Williams, D.L. Hawkins, Sound generation by turbulence and surface in arbitrary motion, *Philosophical Transactions of the Royal Society of London A* 264 (1969) 321–342.
- [32] S. Moreau, M. Roger, Back-scattering correction and further extensions of Amiet's trailing edge noise model. Part 2: Applications, *Journal of Sound and Vibration* 323 (2) (2009).
- [33] M. Roger, S. Moreau, K. Kucukcoskun, On sound scattering by rigid edges and wedges in a flow, with applications to high-lift device aeroacoustics, *Journal of Sound and Vibration* 362 (2016) 252–275.
- [34] D.S. Jones, Aerodynamic sound due to a source near a half-plane, *IMA Journal of Applied Mathematics* 9 (1) (1972) 114–122.
- [35] S.W. Rienstra, Sound diffraction at a trailing edge, *Journal of Fluid Mechanics* 108 (1981) 443–460.
- [36] M. Roger, S. Moreau, Edge scattering of distributed sources—application to high-lift device noise, *14th AIAA/CEAS Aeroacoustics Conference*, AIAA Paper 2008-2866, Vancouver, Canada, 2008.
- [37] R.K. Amiet, Effect of the incident surface pressure field on noise due to turbulent flow past a trailing edge, *Journal of Sound and Vibration* 57 (2) (1978) 305–306.
- [38] M. Roger, S. Moreau, Back-scattering correction and further extensions of Amiet's trailing-edge noise model. Part 1: Theory, *Journal of Sound and Vibration* 286 (2005) 477–506.
- [39] M. Abramowitz, I.A. Stegun, *Handbook of Mathematical Functions: With Formulas, Graphs, and Mathematical Tables*, no. 55, Courier Corporation, 1964, Dover Publications, Inc., New York.
- [40] I.S. Gradshteyn, I.M. Ryzhik, *Table of Integrals, Series, and Products*, Academic Press, New York, 1980.
- [41] R. Mittra, L. Lee, *Analytical Techniques in the Theory of Guided Waves*, The MacMillan Company, New York, 1971.
- [42] C.M. Linton, D.V. Evans, Acoustic scattering by an array of parallel plates, *Wave Motion* 18 (1) (1993) 51–65.

- [43] J. Ingenito, M. Roger, Analytical Modelling of Sound Transmission through the Passage of Centrifugal Compressor, AIAA Paper 2007-3704, Rome, Italy, 2007.
- [44] S. Bouley, B. François, M. Roger, H. Posson, S. Moreau, On a mode-matching technique for sound generation and transmission in a linear cascade of outlet guide vanes, *21st AIAA/CEAS Aeroacoustics Conference*, AIAA Paper 2015-2825, Dallas, TX, June 2015.
- [45] M.E. Goldstein, *Aeroacoustics*, McGraw-Hill, New York, 1976.
- [46] Y. Rozenberg, G. Robert, S. Moreau, Wall-pressure spectral model including the adverse pressure gradient effects, *AIAA Journal* 50 (10) (2012) 2168–2179.
- [47] P. Gliebe, R. Mani, H. Shin, B. Mitchell, G. Ashford, S. Salamah, S. Connell, Aeroacoustics Prediction Codes, Contractor Report CR-2000-210244, NASA, 2000.
- [48] A. Guedel, M. Robitu, N. Descharmes, D. Amor, J. Guillard, Prediction of the blade trailing-edge noise of an axial flow fan, *ASME 2011 Turbo Expo: Turbine Technical Conference and Exposition*, American Society of Mechanical Engineers, Vancouver, Canada, 2011, pp. 355–365.
- [49] E.J. Brambley, N. Peake, Sound Transmission in Strongly-Curved Slowly-Varying Cylindrical and Annular Lined Ducts with Flow, AIAA Paper 2006-2582, Cambridge, MA, May 2006.
- [50] U.W. Ganz, P.D. Joppa, T.J. Patten, D.F. Scharpf, Boeing 18-inch Fan Rig Broadband Noise Test, Contractor Report CR-1998-208704, NASA, 1998.
- [51] S.A.L. Glegg, Broadband Fan Noise Generated by Small Scale Turbulence, Contractor Report CR-207752, NASA, 1998.
- [52] Y. Rozenberg, Modélisation analytique du bruit aérodynamique à large bande des machines tournantes: utilisation de calculs moyennés de mécanique des fluides, PhD thesis, Ecole Centrale de Lyon, dcembre 2007, n° ordre: 2007-44.
- [53] R.P. Woodward, C.E. Hughes, R.J. Jeracki, C.J. Miller, Fan Noise Source Diagnostic Test—Far-Field Acoustic Results, Technical Memorandum TM-2002-211591, NASA, May 2002.
- [54] M. Roger, B. François, M. Bauerheim, Three-dimensional modeling of annular cascade trailing-edge noise, *22nd AIAA/CEAS Aeroacoustics Conference*, AIAA Paper 2016-2949, Lyon, France, 2016.
- [55] M. Roger, S. Moreau, A. Marsan, Generation and transmission of spiral acoustic waves in multi-stage subsonic radial compressors, *20th AIAA/CEAS Aeroacoustics Conference*, AIAA Paper 2014-3232, Atlanta, GA, 2014.